

## Article

# Parametric Optimization of Friction Stir Welding of AA6061-T6 Samples Using the Copper Donor Stir-Assisted Material Method

Aiman H. Al-Allaq <sup>1</sup>, Joseph Maniscalco <sup>1</sup>, Srinivasa Naik Bhukya <sup>2</sup>, Zhenhua Wu <sup>2</sup>  
and Abdelmageed Elmustafa <sup>1,\*</sup>

<sup>1</sup> Department of Mechanical and Aerospace Engineering, Old Dominion University, Norfolk, VA 23529, USA; aalal005@odu.edu (A.H.A.-A.); jmani001@odu.edu (J.M.)

<sup>2</sup> Department of Engineering, Virginia State University, Petersburg, VA 23806, USA; sbhukya@vsu.edu (S.N.B.); zwu@vsu.edu (Z.W.)

\* Correspondence: aelmusta@odu.edu

**Abstract:** This study presents an optimization of the process parameters for the effect of copper (Cu) donor material percentage on the friction stir welding (FSW) of AA6061-T6 alloy. Extensive factorial experiments were conducted to determine the significance of the rotational speed ( $\omega$ ), the transverse speed ( $v$ ), the interface coefficient of friction ( $\mu$ ), and the Cu donor material percentage in the plunge, left, right, and downstream zones. Design Expert 13 software was used to identify the number of simulation experiments to be conducted using the Abaqus simulation software. From Design Expert 13, which is a thorough multi-objective optimization analysis software, we were able to identify ideal welding parameters such as a rotational speed of 1222 rpm, transverse speed of 1.1 mm/s, the coefficient of friction of 0.9, and a 19% donor material percentage for the plunge zone. Significant findings demonstrate that increasing the Cu donor material substantially reduced the temperature from 502 °C to 134 °C when the Cu content is increased from 0% to 50%. This integrated modeling and optimization approach provides a practical procedure to identify the best experimental parameters for the process and a new understanding to guide advances for high-quality FSW of aluminum alloys. This work offers a methodology for optimizing the FSW parameters aligned with multifaceted thermomechanical physics.

**Keywords:** CDSA; optimization; simulation



**Citation:** Al-Allaq, A.H.; Maniscalco, J.; Bhukya, S.N.; Wu, Z.; Elmustafa, A. Parametric Optimization of Friction Stir Welding of AA6061-T6 Samples Using the Copper Donor Stir-Assisted Material Method. *Metals* **2024**, *14*, 536. <https://doi.org/10.3390/met14050536>

Academic Editor: Alberto Campagnolo

Received: 4 April 2024  
Revised: 24 April 2024  
Accepted: 29 April 2024  
Published: 30 April 2024



**Copyright:** © 2024 by the authors. Licensee MDPI, Basel, Switzerland. This article is an open access article distributed under the terms and conditions of the Creative Commons Attribution (CC BY) license (<https://creativecommons.org/licenses/by/4.0/>).

## 1. Introduction

Friction stir welding (FSW) has become a cornerstone method for joining metals and alloys, extending its application from low-strength materials to high-strength materials such as steels, owing to its successful outcomes. Aluminum alloys, notably AA6061-T6, are particularly attractive for FSW due to their light weight, corrosion resistance, and malleability, making them ideal for aerospace, automobile engines, and numerous other applications [1]. Despite the process's advantages, concerns around tool wear due to the development of significant frictional forces have prompted research into various mitigation strategies, including advanced tool designs [2] and the introduction of additional heating sources [3].

Efforts to refine friction stir welding (FSW) have led researchers to explore various techniques for optimizing welding parameters. Ghaffarpour et al. [4] and Salah et al. [5] employed response surface methodology (RSM) to identify optimal parameter configurations that balance mechanical properties and process efficiency. This approach has proven essential in advancing FSW technology across diverse industrial applications. Similarly, Pandiyarajan and Marimuthu [6] demonstrated the effectiveness of the Box–Behnken design in enhancing the tensile characteristics of aluminum composites, further highlighting the importance of systematic parameter optimization.

In addition to the focus on parameter optimization, several studies have addressed the challenges associated with welding dissimilar aluminum alloys. Palanivel and Koshy Mathews [7], Verma and Kumar [8], Ghaffarpour et al. [9], and Sabry et al. [10] investigated the complex interactions resulting from the diverse material properties of various aluminum alloys. These studies emphasized the critical need for systematic parameter optimization in FSW to achieve high-quality joints when welding dissimilar materials.

Recent studies have significantly advanced our understanding of FSW by investigating the role of process parameters in achieving weld quality. Madani et al. [11], Tinguery et al. [12], Iqbal et al. [13], Schmidt and Hattel [14], and Maneiah et al. [15] explored parameter optimization, microstructure evolution, thermomechanical conditions, and tensile strength in the FSW of various aluminum alloys. Chalurkar and Shukla [16], Sharma et al. [17], Sefene et al. [18], and Raturi and Bhattacharya [19] examined temperature fields, experimental studies, multi-criterion optimization, and the local mechanical properties in FSW.

Yue et al. [20], Salih et al. [21], and Lu et al. [22] investigated the tool forces, heat generation, plastic deformation, residual stresses, and temperature fields in the FSW of different aluminum alloys. Jo et al. [23] optimized friction stir spot welding using advanced computational techniques. These studies highlight the importance of systematic parameter optimization in FSW, considering mechanical properties, microstructure, thermal history, tool forces, and environmental sustainability.

The donor stir material concept relies on understanding the heat transfer and material flow interactions that occur between the tool pin, tool shoulder, and the surrounding workpiece material during the friction stir welding process. The donor material is sandwiched between the workpiece and the tool head. The hardness and melting points of the donor stir material are projected to be lower than those of the workpieces' counterparts. The process begins with the tool pin spinning and plunging into the softer donor material. This generates a plastic work zone with a plastic flow surrounding the tool. This plastic work zone remains with the tool pin. It performs as a preheating mechanism that is expected to soften the surrounding material of the workpieces ahead of the tool pin during the welding process. We successfully implemented this concept for the FSW of AA6061-T6 and carbon steel in our studies by Mandal et al. [24], Maniscalco et al. [25], and Bhukya et al. [26].

Further, Al-Allaq et al. [27], using SEM-EDS, XRD, and Nanoindentation, observed Al as the predominant element in the weld, with traces of C, Fe, Mg, Mn, O, and Si, and notably, the absence of the Cu donor material in the stir zone. The stir zone was softer than the base metal for 20% and 60% Cu donor material samples. The stir zone hardness was similar to the AA6061-T6 base material, suggesting that the copper did not impact the final weld hardness as it was depleted during welding, validating the effectiveness of the Cu donor concept in FSW.

Aiming to refine FSW process parameters further, our research integrates the design of experiments (DoE) with simulation techniques. This combination seeks not only to reduce the necessity for extensive physical experimentation, but also to enhance the reliability and effectiveness of FSW, advancing both theoretical knowledge and practical applications in the field.

## 2. Material and Methods

A structured approach to optimize the key welding parameters for FSW of AA6061-T6 alloy, which combines the simulation, design of experiments (DoE), and statistical analysis, was employed in this study. Using the techniques established in previous studies by Mandal et al. and Maniscalco et al. [24,25], the FSW process was modeled in Abaqus. Utilizing the results provided by these simulations, a DoE was created to investigate the effects of various FSW parameters, the rotational speed, the transverse speed, the coefficient of friction, and the Cu donor material percentage, on the process outcomes, explicitly focusing on axial force and temperature as response variables. The DoE was then executed within the Abaqus environment to simulate these responses under different input parameter settings.

Finally, the data from these simulations were analyzed using Design Expert 13 software [28], where the analysis of variance (ANOVA) and optimization techniques were applied to identify the optimal welding parameters. This strategy supplements the conventional DoE by deliberately reducing the number of experimental runs required while gathering essential data points. It specifically addresses the problem of managing many variables in FSW, an intrinsically rich process in interconnections and possible complications.

Generally, the three main randomized categories for the response surface designs are central composite, Box–Behnken, and optimal. The Box–Behnken category only requires 3 levels. The most accurate one is central composite designs (CCD). CCD can be used with 5 and 3 levels of input data.

The simulations assessed an AA6061-T6 plate under three conditions: (1) no Cu donor material, (2) with 25% Cu donor material, and (3) with 50% Cu donor material, respectively. Rotational speeds of 1200, 1300, 1400, and 1500 rpm were explored, while transverse speeds of 1, 2, 3, and 4 mm/s were considered. Furthermore, the coefficients of friction of 0.3, 0.4, 0.5, and 1.0 were incorporated in the simulations, as detailed in the work presented in [25].

### 3. Finite Element Models of the Donor Stir Material FSW Simulation

In this research, we adopted the elasto-plastic Johnson–Cook material constitutive model built-in Abaqus finite element code to simulate various FSW cases. These simulations expanded the earlier work of Maniscalco et al. by including the optimization of several FSW parameters such as transverse welding speed, rotational speed, Cu donor material percentage, and the coefficient of friction [25]. The workpiece meshed with 8-node-coupled temperature-displacement brick elements (C3D8RT), and the tool was assumed to be rigid with the dimensions shown in Figure 1. The tool pin was modeled as a straight cylindrical pin as opposed to the various complicated geometries that are traditionally used in experiments to simplify the FEM. The mesh density was increased around the tool plunge area with 19,200 elements to produce accurate simulation results, particularly in areas with high thermal and mechanical interactions [25]. The workpiece was constrained along the sides, so there was no deformation, except for compression in the tool plunge direction. The bottom surface was also constrained to prevent the bending of the surface.

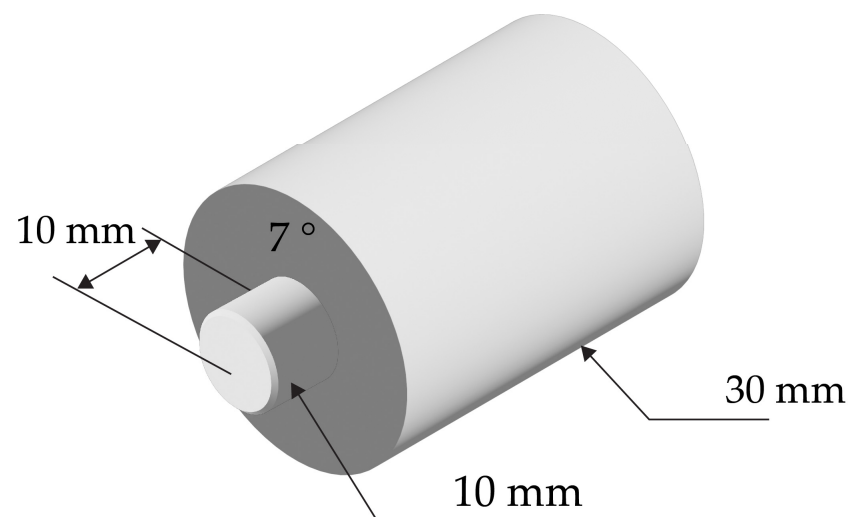


**Figure 1.** Tool design used in the simulation.

Our model integrates Cu thermal interactions with AA6061-T6, using expanded 3D Explicit Abaqus simulation results as the input for our optimization. Using a Coulomb coefficient of friction, backed by Mandal's experiments, provided a reasonable friction approximation for our initial simulations, balancing accuracy with complexity [24]. The simulation results for optimizing the parameters listed above are shown during the plunge and the welding processes for the Al plate with no donor material and after placing and

engaging the 25 and 50% Cu donor material on top of the Al plate. Table 1 summarizes the tools and methods used.

**Table 1.** Tools and methods.

Parameter	Details
Materials	Al6061-T6 parent, Cu donor
Tool geometry	30 mm shoulder diameter, 10 mm pin diameter, 10 mm pin length
Boundary conditions	The sides are constrained against transverse deformation, and the bottom is fixed.
Interactions	Thermal and mechanical coupling at interfaces
Mesh	Brick elements (C3D8RT), refined in the weld zone
Elements	19,200 elements
Constitutive model	Johnson-Cook elasto-plastic
Friction model	Coulomb coefficient of friction

#### 4. Modeling

Table 2 describes the DoE parameters used in optimizing the FSW study. The list in Table 2, which includes the rotational speed, transverse speed, the coefficient of friction, and donor material percentages, underlines the impact of varying these process parameters on the weld's ultimate quality, strength, and efficiency. By systematically executing these 16 distinct experimental runs, optimal combinations of rotational speed, transverse speed, the coefficient of friction, and Cu donor material percentage were reached, which are expected to produce desirable weld outcomes.

**Table 2.** Design of the experiment parameters for FSW optimization.

Run	$\omega$ (rpm)	$v$ (mm/s)	$\mu$	$D$
1	1200	1	0.3	50
2	1200	1	1	0
3	1200	2	0.7	25
4	1200	3	1	50
5	1200	4	0.5	50
6	1200	4	0.3	0
7	1300	1	0.5	0
8	1300	1	1	50
9	1300	3	0.3	25
10	1300	4	1	25
11	1400	3	0.7	0
12	1500	1	1	50
13	1500	1	1	25
14	1500	2	0.3	0
15	1500	2	0.5	25
16	1300	3	0.3	25
17	1500	3	1	50
18	1500	4	0.5	25

For instance, the third experimental condition is characterized by a rotational speed of 1200 rpm, a transverse speed of 2 mm/s, a coefficient of friction of 0.7, and 25% of the Cu donor material. In contrast, the seventeenth experimental condition is described by a rotational speed of 1500 rpm, a transverse speed of 3 mm/s, a coefficient of friction of 1.0, and a higher Cu donor material percentage of 50. This ensures a comprehensive and meaningful exploration of the process conditions. Consequently, this table serves as a solid foundation for the entire experimental design, enabling detailed analysis and optimization of the FSW process. Table 3 lists the extremes, i.e., the maximum and minimum values, for each of the four parameters under study.

**Table 3.** The maximum and minimum levels of evaluated factors.

Name	Units	Min	Max
$\omega$	rpm	1200	1500
$v$	mm/s	1	4
$\mu$		0.3	1
$D$	%	0	50

## 5. Simulation Analysis

The optimal design method was performed to determine the effect of process parameters on the response parameters. The simulation results that describe this optimization method are presented for the four separate regions identified in Figure 2. Figure 2a represents a 3D model, highlighting the donor and parent materials, depicting the advancing and retreating sides of the tool's rotation. This distinction is crucial as temperatures typically vary between the advancing and retreating sides due to differences in the heat generation and material flow dynamics.

In Figure 2b, the plunge zone (PZ) is represented with elements that signify the presence of the Cu donor material. Region 1, identified as the left interface zone (LZ), includes elements in the donor material adjacent to those in the parent material, predominantly located on the advancing side where the heat input and material flow are more intense. Conversely, region 2, denoted as the right interface zone (RZ), comprises elements in the parent material adjacent to the donor material, positioned mainly on the retreating side where the heat input and material dynamics differ. Lastly, region 3, designated as the downstream (DS) region, is characterized by elements in the parent material extending away from the tool's path and experiencing varying thermal and mechanical effects due to the tool's progression. The analysis of variance (ANOVA) was employed to determine the conditions that allow the optimization process and to verify the model's significance or otherwise.

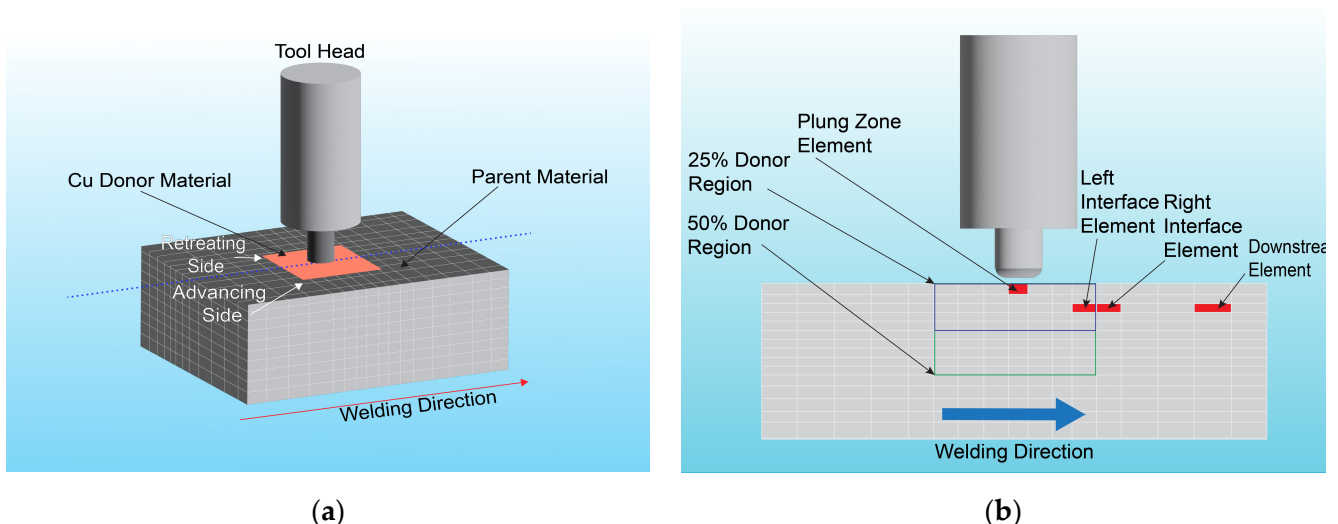


**Figure 2.** (a) A Full model of the donor–parent material. (b) Illustrations of the donor stir and parent material regions.

Figure 3 incorporates two detailed ABAQUS simulation plots to demonstrate the temperature distribution at the end of the welding stage, specifically for the condition of 1400 rpm and 3 mm/sec travel speed with fine meshes. A pure Lagrangian approach was adopted for the simulation, which resulted in solution convergence and prevented premature termination caused by excessive element distortion. These plots distinctly compare 25% and 50% Cu donor material scenarios in an aluminum-base material. Intriguingly,

our findings reveal a striking similarity in the temperature distribution for both donor material percentages, indicating that variations in copper content within this range do not substantially alter the thermal profile at this welding stage. This consistency in temperature distribution, regardless of the Cu percentage, is a critical insight, suggesting the feasibility of achieving consistent weld quality while leveraging the benefits of Cu as a donor material in friction stir welding.

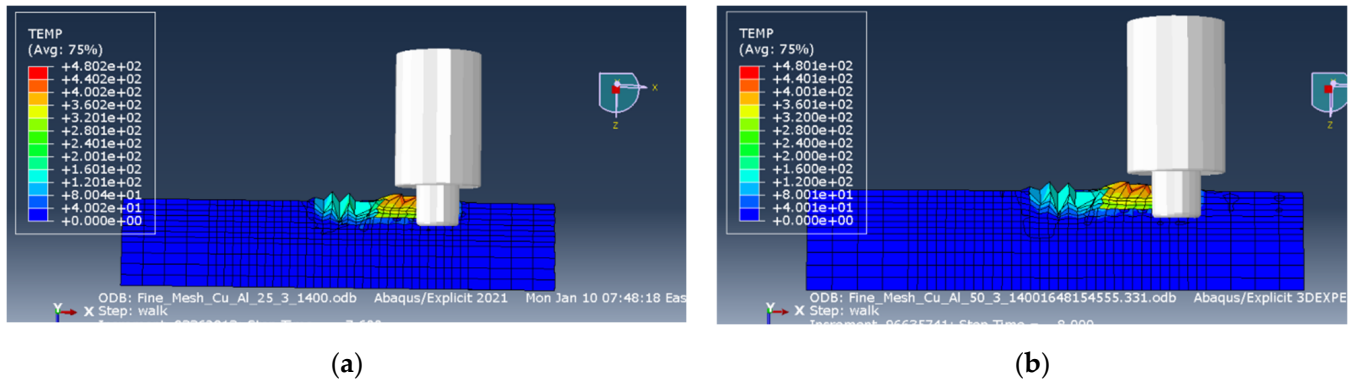


**Figure 3.** (a) Temperature distribution of the 1400 rpm and 3 mm/s travel speed fine meshes for 25% Cu donor material (b) Temperature distribution of the 1400 rpm and 3 mm/s travel speed fine meshes for 50% Cu donor material.

## 6. Results

The numerical simulations were conducted using Abaqus. Table 4 summarizes the predicted axial force and temperature in the plunge zone of the weld. The plunge zone is the initial phase of the welding process, where the tool penetrates the Cu donor material and the workpiece. The Cu donor material is fastened to the top of the workpiece. The axial force values varied between 1962 N and 3346 N (an average of 2755 N), and the temperature values varied between 135 °C and 502 °C (an average of 330 °C), respectively. Notably, the axial force's higher values correspond to a greater tool penetration force, affecting the tool's lifespan and energy consumption. At the same time, temperature is a critical parameter influencing the material flow and the resulting weld properties. The unique thermal and mechanical characteristics of Cu, such as its exceptional thermal conductivity and response to high temperatures, can substantially impact the temperature distribution and the material's softening during welding.

**Table 4.** Simulation results for the plunge zone (PZ).

Response	Mean (Overall)
Response 1, $P$ (N)	2755
Response 2, $T$ (°C)	330

Table 5 presents the axial force and temperature results for the left zone of the weld. This zone, adjacent to the plunge, also plays a significant role in determining the quality of the weld, with values averaging around 3067 N for the axial force and 171 °C for temperature. It is noted that a high axial force may indicate a greater level of deformation occurring in the weld. The extensive temperature range displayed in the table is pivotal, as it directly influences the thermal and mechanical properties of the weld and, consequently, the weld's final structure.

**Table 5.** Simulation results for the left zone (LZ).

Response	Mean (Overall)
Response 1, $P$ (N)	3067
Response 2, $T$ ( $^{\circ}\text{C}$ )	171

Transitioning to Table 6, data from the right zone of the weld are displayed—this region mirrors the left zone. Here, the average value of the axial force is around 1804 N, and the average temperature is 250  $^{\circ}\text{C}$ .

**Table 6.** Simulation results for the right zone (RZ).

Response	Mean (Overall)
Response 1, $P$ (N)	1804
Response 2, $T$ ( $^{\circ}\text{C}$ )	250

Finally, Table 7 outlines the axial force and temperature results for the downstream zone of the weld, a region of high significance as it represents the final path of the FSW tool. The range of the axial force in this zone averages about 1726 N from 188 N to 7018 N, and the temperature fluctuates around 113  $^{\circ}\text{C}$ , given that this region represents the closure of the stir zone, where a defect-free weld is paramount.

**Table 7.** Simulation results for the downstream zone (DS).

Response	Mean (Overall)
Response 1, $P$ (N)	1726
Response 2, $T$ ( $^{\circ}\text{C}$ )	113

The simulation results outlined in Tables 4–7 represent a thorough understanding of the axial force and temperature variations across different weld zones during the FSW process [16]. The response data were then used as input parameters into the Design Expert 13 software for statistical evaluation and to develop modeling outcomes. The chosen model for each response was determined by evaluating the goodness-of-fit provided by the ANOVA (analysis of variance) results. Tables 7–9 constitute the foundational bridge from the raw simulation results to their practical application in predictive models for each FSW zone’s axial force and temperature.

**Table 8.** Integrated ANOVA table for plunge zone force and temperature models.

Source	F-Value (Force)	$p$ -Value (Force)	F-Value (Temperature)	$p$ -Value (Temperature)
Model	5.85	0.0087	56.63	<0.0001
$\omega$	0.02	0.9030	1.22	0.3013
$v$	0.25	0.6349	2.83	0.1312
$\mu$	12.58	0.0062	303.06	<0.0001
$D$	1.09	0.3231	169.98	<0.0001
$\omega\mu$	5.25	0.0477	8.19	0.0211
$v\mu$	5.97	0.0371	-	-
$\mu^2$	4.56	0.0615	-	-
$\omega D$	-	-	7.78	0.0236
$D^2$	-	-	10.16	0.0129

The analysis of variance (ANOVA) results in Table 8 for the reduced quadratic model of the axial force in the plunge zone showed that the coefficient of friction is the most significant factor. This aligns with the very low  $p$ -value of 0.0062 and high  $F$ -value of 12.58.

The model explains a considerable variance, as seen by an  $R^2$  of 0.85, indicating that it captured most of the plunge zone force response variation.

**Table 9.** Integrated ANOVA table for the left zone force and temperature models.

Source	F-Value (Force)	p-Value (Force)	F-Value (Temperature)	p-Value (Temperature)
Model	87.00	0.0018	36.05	0.0273
$\omega$	61.90	0.0043	2.13	0.2823
$v$	1.42	0.3191	167.37	0.0059
$\mu$	444.34	0.0002	106.24	0.0093
D	339.25	0.0003	140.12	0.0071
$\omega v$	59.09	0.0046	12.17	0.0732
$\omega \mu$	58.87	0.0046	0.29	0.6468
$\omega D$	-	-	17.22	0.0535
$v \mu$	22.89	0.0174	16.07	0.0570
$v D$	-	-	43.90	0.0220
$\mu D$	-	-	0.10	0.8057
$\omega^2$	-	-	8.52	0.1001
$v^2$	6.47	0.0844	3.08	0.2213
$\mu^2$	10.58	0.0474	3.53	0.2011
$D^2$	-	-	29.80	0.0320
$\omega v \mu$	168.47	0.0010	-	-
$\omega \mu^2$	88.37	0.0026	-	-
$v^2 \mu$	252.92	0.0005	-	-
$v \mu^2$	11.63	0.0421	-	-

In Equation (1), the corresponding fitted model relates the input factors (rotational speed  $\omega$ , transverse speed  $v$ , the coefficient of friction  $\mu$ , and Cu donor material percentage D) to the plunge zone force ( $P_{\text{plunge}}$ ). The factor of 9842, which is the trailing mu, indicated that the coefficient of friction possesses a more dominant effect than the other factors. Using this equation, increasing the coefficient of friction from its minimum of 0.3 to a maximum of 1.0 increases the predicted plunge force from around 2907 N to 3346 N.

$$P_{\text{plunge}} = 2.9\omega + 281.8v + 9842.4\mu - 3.1D - 4.3\omega\mu - 476.2v\mu - 2863.4\mu^2 - 2097.6 \quad (1)$$

For the plunge zone temperature, the Cu donor material percentage is the most significant parameter based on its remarkably low p-value of less than 0.0001 and very high F-value of 169.98. The fitted parameters in (Equation (2)) contain a Cu donor material percentage trailing factor of 3.27, which is associated with its significance. This model predicts that increasing the Cu donor material content from 0% to 50% decreases the temperature ( $T_{\text{plunge}}$ ) in the plunge zone from 502 °C to 134 °C due to the improved conductivity.

$$T_{\text{plunge}} = -0.2\omega + 22.3 - 392.1\mu + 3.3D + 0.5\omega\mu - 0.01\omega D + 46.5v\mu + 0.06D^2 + 481.2 \quad (2)$$

In the left zone, the axial force response in Table 9 is significantly influenced by the Cu donor material percentage, as evidenced by a low p-value of 0.0003 and a high F-value of 339.25. The 0.97  $R^2$  value shows an excellent model fit.

Equation (3) depicts a trailing factor of 78.8 for the Cu donor material percentage; which is smaller than the trailing factor of the coefficient of friction but is still significant in magnitude.

$$P_{\text{Left}} = 2.9\omega + 4659.5v - 89176.7\mu + 78.8D - 21.6\omega v + 96.1\omega\mu - 65110.9v\mu - 3365.2v^2 + 1.3E^5\mu^2 + 26\omega v\mu - 109.7\omega\mu^2 + 4870.4\mu v^2 + 5341.2v\mu^2 - 21818.5 \quad (3)$$

In Equation (4), the Cu donor material percentage remains important for the left zone temperature ( $T_{Left}$ ), but the transverse speed is considered the most significant factor. The Cu donor material percentage still has a low p-value of 0.0071 and a high F-value of 140.12, confirming that it strongly influences the temperature results. The quadratic model fit is good, with an  $R^2$  of 0.96.

$$T_{Left} = -3.7\omega + 314.9v - 22.9\mu + 11.7D - 0.2\omega v - 0.1\omega\mu - 0.01\omega D + 69.2v\mu - 1.6vD - 0.4\mu D + 0.002\omega^2 - 9.9v^2 + 198.4\mu^2 + 0.1D^2 + 1918.5 \quad (4)$$

In the ANOVA results of Table 10 for the axial force in the right zone, the Cu donor material percentage is becoming less significant, as seen by its higher p-value of 0.6374 and lower F-value of 0.26. The cubic model fit indicates an  $R^2$  value of 0.83, which is not significantly high and represents some uncertainties.

**Table 10.** Integrated ANOVA table for right zone force and temperature models.

Source	F-Value (Force)	p-Value (Force)	F-Value (Temperature)	p-Value (Temperature)
Model	19.20	0.0058	27.79	0.0001
$\omega$	-	-	0.10	0.7559
$v$	4.11	0.1127	135.98	< 0.0001
$\mu$	121.25	0.0004	49.32	0.0002
$D$	0.26	0.6374	5.24	0.0560
$\omega v$	3.50	0.1349	18.97	0.0033
$\omega\mu$	11.36	0.0280	4.79	0.0647
$v\mu$	32.57	0.0047	23.07	0.0020
$vD$	20.99	0.0102	9.56	0.0175
$\mu D$	11.98	0.0258	-	-
$\mu^2$	5.67	0.0759	3.53	0.2011
$D^2$	63.54	0.0013	29.80	0.0320
$\omega v\mu$	31.35	0.0050	-	-
$\omega^2$	-	-	11.96	0.0106

Equation (5), the factor of  $-120$  trailing the Cu donor material percentage, indicates the minimal influence of the Cu donor material on the force in the right zone ( $P_{Right}$ ).

$$P_{Right} = -17.4\omega - 11475.4v - 23642.6\mu - 120.4D + -9.5\omega v + 24.7\omega\mu + 16038.2v\mu + 15.9vD - 56.4\mu D - 9.9v^2 + 3553.4\mu^2 + 2.2D^2 - 12.9\omega v\mu + 20661.6 \quad (5)$$

In Equation (6), the factor of  $1.8$  trailing the Cu donor material percentage represents a decrease in temperature in the right zone ( $T_{Right}$ ) in comparison to the factor of  $11.7$  in the left zone, as explained in Equation (4). This is an expected outcome of the heat transfer from the plunge zone to the left zone and eventually to the right zone. We expect this to result in enough heat transfer to loosen the material ahead of the tool pin.

$$T_{Right} = -8.3\omega - 407v + 712.7\mu + 1.8D - 0.3\omega v - 0.6\omega\mu + 133v\mu - 1.2vD - 56.4\mu D - 0.004\omega^2 + 4892.3 \quad (6)$$

The downstream zone presents a unique scenario in which the Cu donor material percentage's effect on axial force and temperature is relatively less significant compared to other factors like transverse speed, as shown by Equations (7) and (8). This is a significant outcome, as we predicted that the Cu donor material would cease to exist in the downstream zone during welding.

$$P_{Downstream} = -127.3\omega + 270v + 3583.1\mu - 46.3D - 1473.5\mu v - 1561.2vD + 0.05\omega^2 + 471.1v^2 + 1.3D^2 + 83936 \quad (7)$$

$$T_{\text{Downstream}} = -10.9\omega - 254.1v - 323\mu + 4.6D + 0.17\omega v + 0.6\omega\mu - 0.01\omega D - 0.2v\mu - 0.01vD + 5.3\mu D + 0.004\omega^2 + 24.2v^2 - 367.3\mu^2 + 0.03D^2 + 7640.2 \quad (8)$$

The desirability approach allows for the identification of the ideal combination of friction stir welding (FSW) process parameters that maximize “desirability” towards meeting the specified goals. Table 11 lists the goals to minimize the axial force and restrict the temperature within set limits across the plunge, left, right, and downstream zones. According to Design Expert 13 software, a high significance of 4 indicates that these responses are equally important.

**Table 11.** Integrated table of input parameters for the desirability function method.

Zone	Response	Goal	Lower Limit	Upper Limit	Significance
Plunge zone	Axial force	Minimize	1962 N	3346 N	4
	Temperature	Range	135 °C	502 °C	4
Left zone	Axial force	Minimize	416 N	7055 N	4
	Temperature	Range	24 °C	364 °C	4
Right zone	Axial force	Minimize	336 N	3911 N	4
	Temperature	Range	44 °C	502 °C	4
Downstream zone	Axial force	Minimize	188 N	7018 N	4
	Temperature	Range	1 °C	318 °C	4

Table 12 provides the optimized input factor levels and the corresponding predicted responses that resulted in the maximum desirability level of 1 for all zones. For example, the optimal predicted parameters in the plunge zone for the four parameters, i.e., rotational speed, transverse speed, the coefficient of friction, and Cu donor material percentage, are 1222 rpm, 1.1 mm/s, 0.9, and 19%, respectively. Furthermore, the predicted optimized parameters for the left zone are 1200 rpm, 3.4 mm/s, 0.9, and 48%, respectively. Since the Cu donor material presence is only restricted to the plunge zone, there should be no Cu donor material in the left, right, or downstream zones. The values of 48, 35, and 48% Cu donor material refer to the Cu donor material in the plunge zone, not in these zones. We initially postulate that the Cu donor material will not be transferred during the welding process as this will produce an inhomogeneous weaker weld. In the experiments, we designed a small groove to house the Cu donor material and used set screws to anchor it to the workpiece. This will ensure that the Cu donor material will not travel with the tool pin during the welding process. We adopted a similar principle in the simulation by restricting the Cu donor material to the plunge zone only.

**Table 12.** Optimal values of setting factors and response variables.

Factor	Plunge Zone	Left Zone	Right Zone	Downstream Zone
$\omega$	1222	1200	1237	1212
$v$	1.1	3.4	3.3	3.8
$\mu$	0.9	0.9	0.8	1
$D$	19%	48%	35%	48%
$P$ (N)	2920	2716	2007	2468
$T$ (°C)	404	300	383	301
<i>Desirability</i>	1	1	1	1

The optimal parameters in Table 12 were determined for each zone independently. However, in a continuous FSW process, the tool moves from the plunge region into the left, right, and the downstream zone.

For instance, the plunge region requires a lower rotational speed of 1222 rpm and a transverse speed of 1.1 mm/s for proper heating and deformation during tool penetration. Meanwhile, the left and downstream zones require higher transverse speeds, between

3.4–3.8 mm/s, for adequate stirring and bonding. Based on these values, a transverse speed of 2–3 mm/s, a rotational speed between 1200–1222 rpm, a coefficient of friction between 0.8–0.9, and a Cu donor material percentage between 19–48%, which is only restricted to the plunge zone, should produce an optimal FSW of the AA6061-T6 plate.

## 7. Discussion of Results

### 7.1. Force Analysis: Plunge, Right, and Downstream Forces

The axial force analysis in the plunge, right, and downstream zones is key for understanding the weld quality of FSW. Lower axial forces indicate efficient tool penetration in the plunge zone, which is essential for reducing the initial weld defects. Our objective was to optimize process parameters by minimizing these forces, enhancing welding efficiency, and reducing tool wear.

In the subsequent zones (left, right, and downstream), optimal force levels ensure uniform material flow, which is critical for achieving homogenous welds with desirable mechanical properties. Adjustments in rotational and transverse welding speeds are critical in balancing material flow and axial force, directly influencing weld quality.

Our findings align with those by Bhukya et al. [26], providing empirical support for the critical impact of controlled axial forces on weld integrity.

#### Relationship between Forces and FSW Process Parameters

The force response surface plots shown in Figures 4–7 offer a helpful visual representation of how the critical FSW parameters impact the axial force in various weld zones.

The axial force is plotted along the vertical axis in Figures 4–7, whereas the input parameters were interchanged between the two other axes.

Figure 4 shows that the axial force is most strongly influenced by the coefficient of friction and the Cu donor material percentage for the critical plunge zone. The surface plots in Figure 4d indicate that the axial force increases with an increase in the coefficient of friction in the plunge zone except when the coefficient of friction approaches 0.9–1.0. With an increase in the Cu donor material percentage, we observe that the axial force drops as the Cu donor material percentage increases and the coefficient of friction increases.

In the left zone, and based on the relationship between the axial force and the control input parameters as given by Equation (3) and the construction of Figure 5a,b,f, we observe that the most dominant parameters are the rotational speed and the coefficient of friction, illustrating that the force is primarily influenced by the rotation speed, followed by the coefficient of friction Figure 5d,e,f. Increasing the rotational speed generates higher axial forces, while increasing the coefficient of friction reduces the axial force. This matches the modeling results where the rotational speed and the coefficient of friction were significant (Equation (3)).

Figure 6a depicts minor axial force changes with the rotation or transverse speeds. Figure 6b shows that increasing the rotational speed and the Cu donor material increases the axial force due to enhanced stirring and heating in the right zone. In Figure 6c, increasing the Cu donor percentage and the transverse speed increases the axial force due to excessive deformation within the right zone. In Figure 6d, we observe that an increase in the Cu donor material percentage in the plunge zone causes the axial force to increase due to the generated stirring pressure. However, a higher coefficient of friction above 0.8 and a moderate Cu donor material percentage reduce the axial force due to less heating and softening. In Figure 6e, larger transverse speeds paired with an increased coefficient of friction decrease the axial force due to material softening. Finally, Figure 6f shows that the rotational speed and the coefficient of friction do not simultaneously or consequentially influence the axial force. In summary, each of the controlling parameters affects the axial force in its way, although we might see two or more influence the axial force collectively, i.e., more Cu donor material percentage and rotational speed increase the axial force (Figure 6b). For example, a higher coefficient of friction combined with transverse speed decreases the axial force via softening (Figure 6d,e).

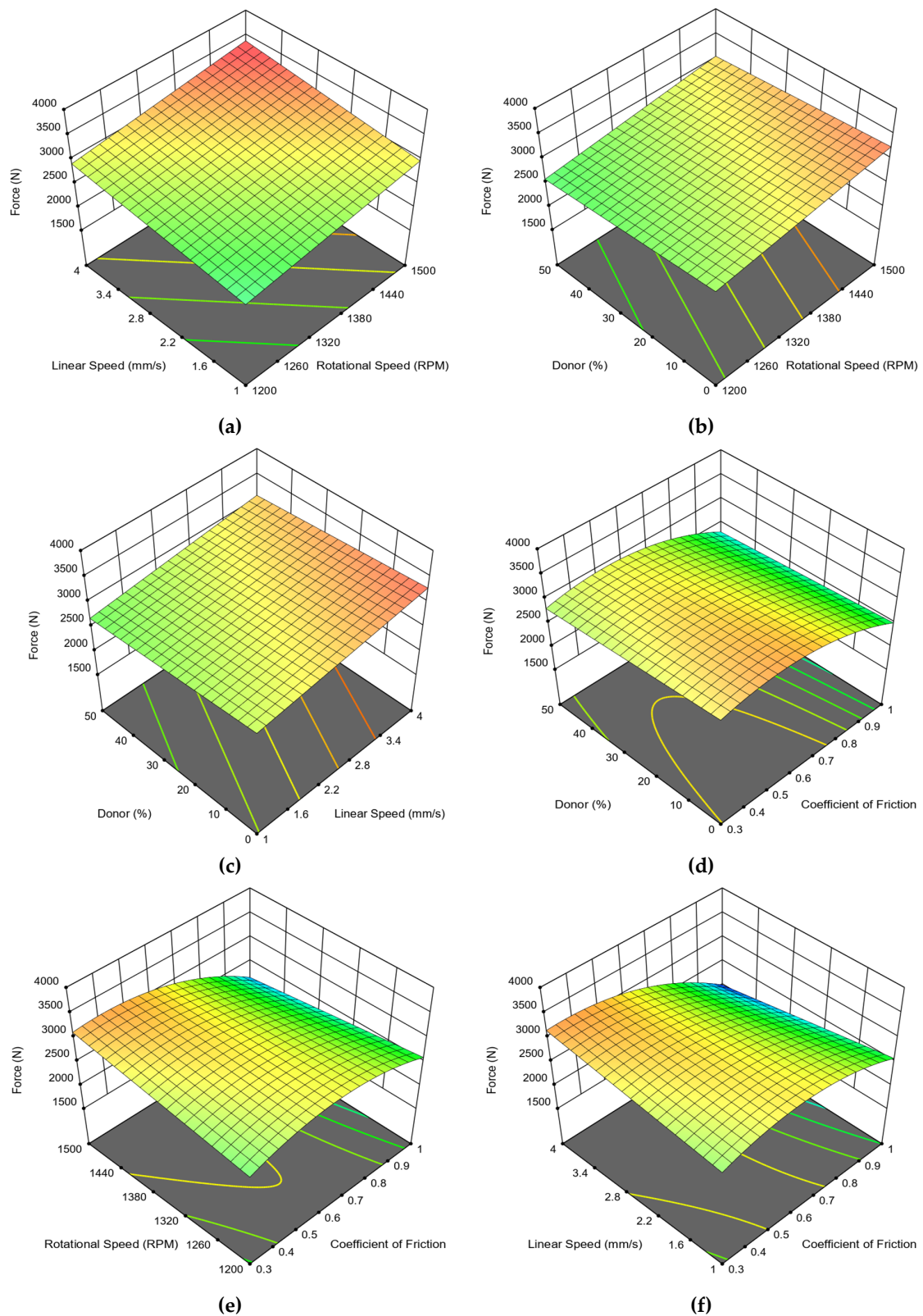


**Figure 4.** Plunge zone force response to varying input factors in FSW. (a) Axial force versus rotational and transverse speeds. (b) Axial force against the Cu donor material percentage and rotational speed. (c) Axial force against the Cu donor material percentage and transverse speed. (d) Axial force against the Cu donor material percentage and the coefficient of friction. (e) Axial force against the rotational speed and the coefficient of friction. (f) Axial force against the transverse speed and the coefficient of friction.

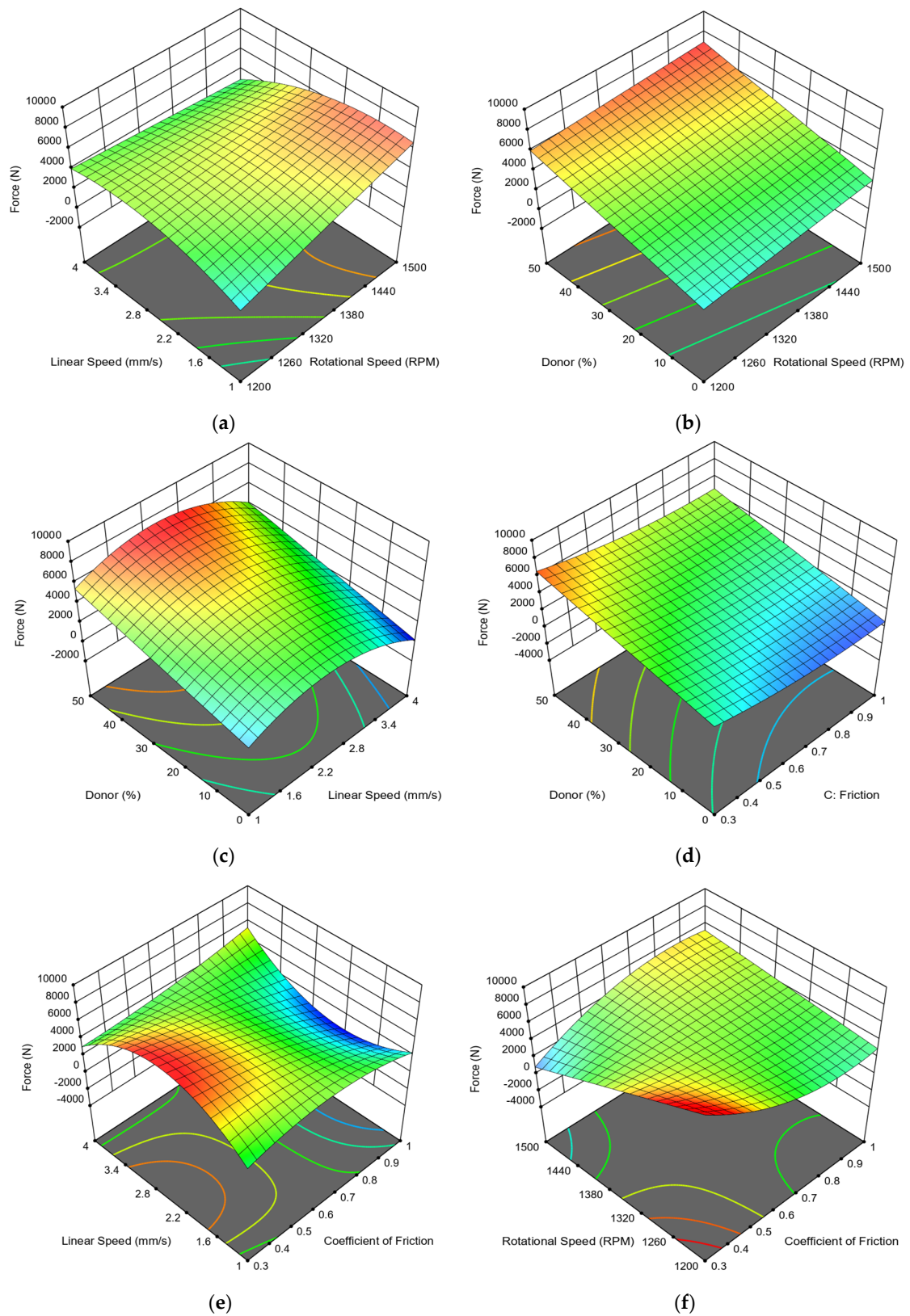


**Figure 5.** Left zone force response to varying input factors in FSW. (a) Axial force versus the rotational and transverse speeds. (b) Axial force against the Cu donor material percentage and rotational speed. (c) Axial force against the Cu donor material percentage and transverse speed. (d) Axial force against the Cu donor material percentage and the coefficient of friction. (e) Axial force against the rotational speed and the coefficient of friction. (f) Axial force against the transverse speed and the coefficient of friction.

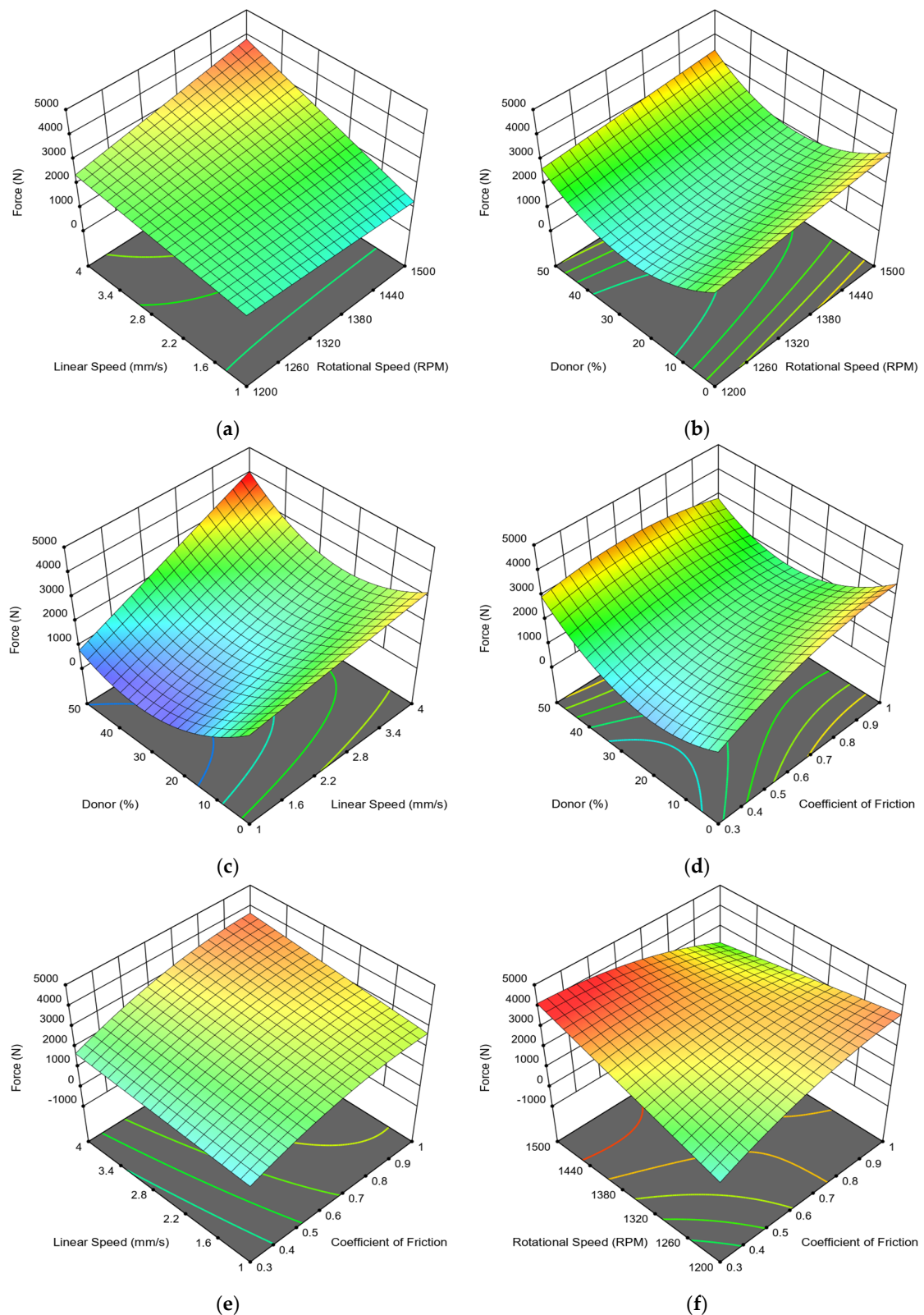


**Figure 6.** Right zone force response to varying input factors in FSW. (a) Axial force versus the rotational and transverse speeds. (b) Axial force against the Cu donor material percentage and rotational speed. (c) Axial force against the Cu donor material percentage and transverse speed. (d) Axial force against the Cu donor material percentage and coefficient of friction. (e) Axial force against the rotational speed and the coefficient of friction. (f) Axial force against transverse speed and the coefficient of friction.

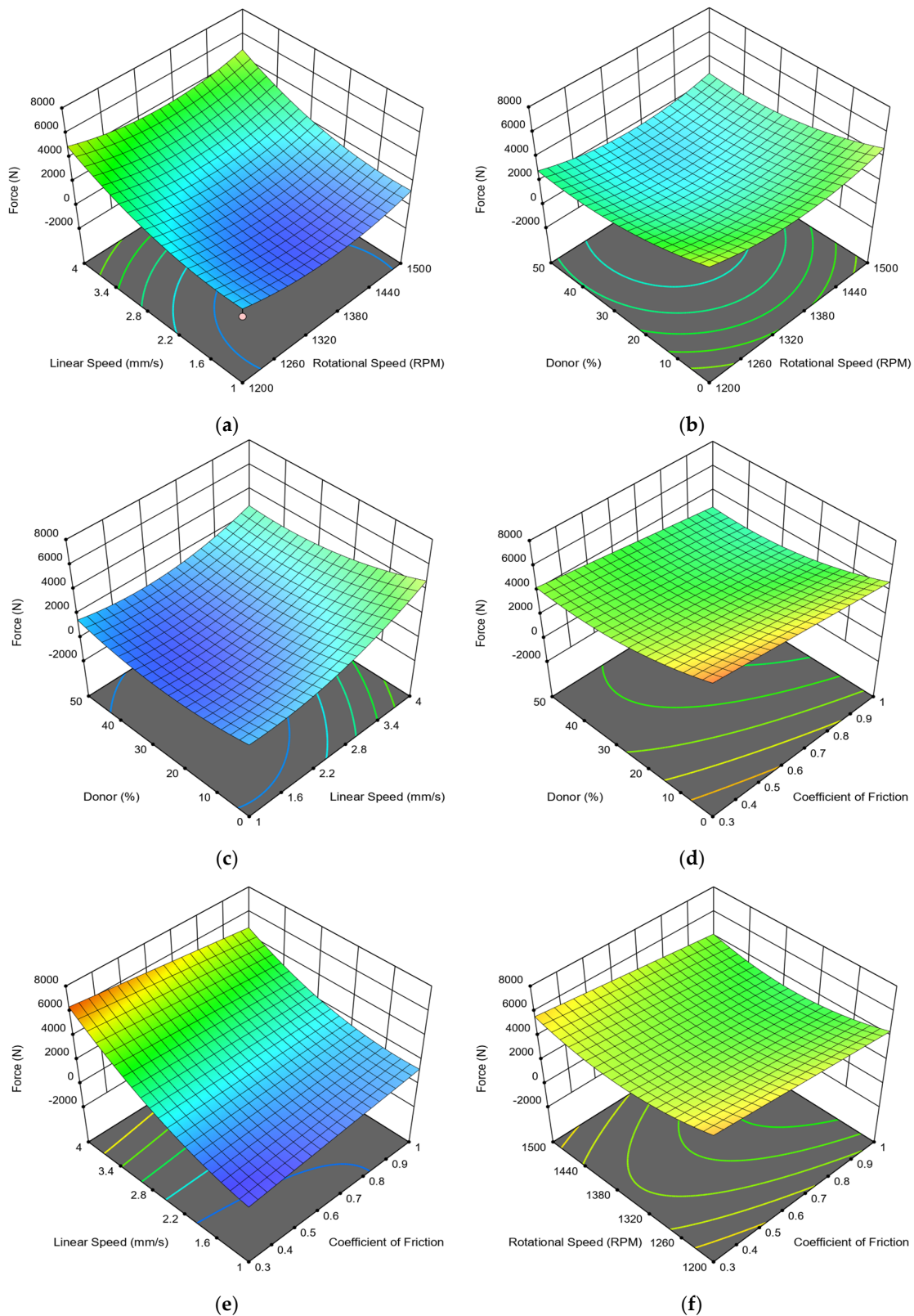


**Figure 7.** Downstream zone force response to varying input factors in FSW. (a) Axial force versus the rotational and transverse speeds. (b) Axial force against the Cu donor material percentage and rotational speed. (c) Axial force against the Cu donor material percentage and transverse speed. (d) Axial force against the Cu donor material percentage and the coefficient of friction. (e) Axial force against the rotational speed and the coefficient of friction. (f) Axial force against the transverse speed and the coefficient of friction.

Figure 7a shows axial force variations with transverse speed and rotational velocity, which indicates a strong dependence only on the transverse speed, with minimal force changes across the range of rotational speeds. This aligns with the model that states that speed dominates (Equation (7)). Figure 7b depicts the response surface concerning Cu donor material percentage and rotational speed. Negligible force changes again confirm that these factors weakly impact forces, as predicted. Figure 7c plots force against transverse speed and Cu donor percentage, revealing that the axial force magnitude correlates only with changes in transverse velocity, while Cu donor material percentages do not alter forces appreciably. Figure 7d conveys a similar dramatic axial force enhancement solely through a higher coefficient of friction, with minimal Cu donor material effects. This reinforces the minimal influence of the Cu donor material content on the downstream zone force. Studying Figure 7e as a function of the coefficient of friction and transverse speed reaffirms conclusions from prior plot-force magnitudes intensify exclusively with transverse speed, not friction values. Lastly, Figure 7f shows a flat response surface, substantiating the lack of collective effects of rotational speed and friction coefficient.

### 7.2. Temperature Analysis: Plunge, Right, and Downstream Zone Temperatures

The optimization analysis and Abaqus simulations showed that the temperature at the plunge, right, and downstream zones decreased as the Cu donor material percentage increased.

#### Relationship between Temperatures and FSW Process Parameters

Figures 8–11 depict the plots of the temperature versus the four input parameters (transverse speed, rotational speed, the coefficient of friction, and Cu donor material percentage) for the plunge zone (Figure 8), left zone (Figure 9), right zone (Figure 10), and downstream zone (Figure 11). Figure 8a shows that the rotational and transverse speeds insignificantly vary with temperature. In contrast, Figure 8b reveals that lower temperatures result when the rotational speed and the Cu donor percentage increase. The decrease in temperature with increased Cu donor material percentage is likely caused by amplified conduction effects. Figure 8c,d depict that increasing the Cu donor material percentage consistently reduces the temperature irrespective of the transverse speed, which indicates that the Cu donor material enhances conductivity. Meanwhile, the coefficient of friction only minimally affects the plunge zone temperature compared to the donor material percentage. Figure 8e demonstrates that increasing the coefficient of friction values only slightly decreases the temperature, while the dominant effect is due to the Cu donor material percentage. Lastly, Figure 8f shows that the rotational speed, combined with the coefficient of friction, has an insignificant effect on the temperature results.

In Figure 9a, the left zone temperature increases with higher rotational and transverse speeds; however, the transverse speed affects the temperature more than the rotational speed. Figure 9b shows that increasing the Cu donor percentage and rotational speed decreases the left zone temperature response. Figure 9c–e indicate that increasing the Cu donor material percentage in the plunge zone decreases the temperature in the left zone regardless of the transverse speed. Finally, Figure 9f indicates that the rotational speed and the coefficient of friction have little to no effect on the temperature results in the left zone.

In Figure 10a, the right zone temperature increases with the transverse speed. The rotational speed has little or no effect. Figure 10b shows that the temperature slightly declines with increased Cu donor material percentage and the rotational speed. Figure 10c indicates that the temperature increases with an increase in the transverse speed. Figure 10d reveals that increasing the coefficient of friction slightly impacts the temperature. Figure 10e shows an increase in temperature with an increase in the transverse speed. Finally, Figure 10f indicates that the rotational speed and the coefficient of friction have little or no effect on the temperature results in the right zone.

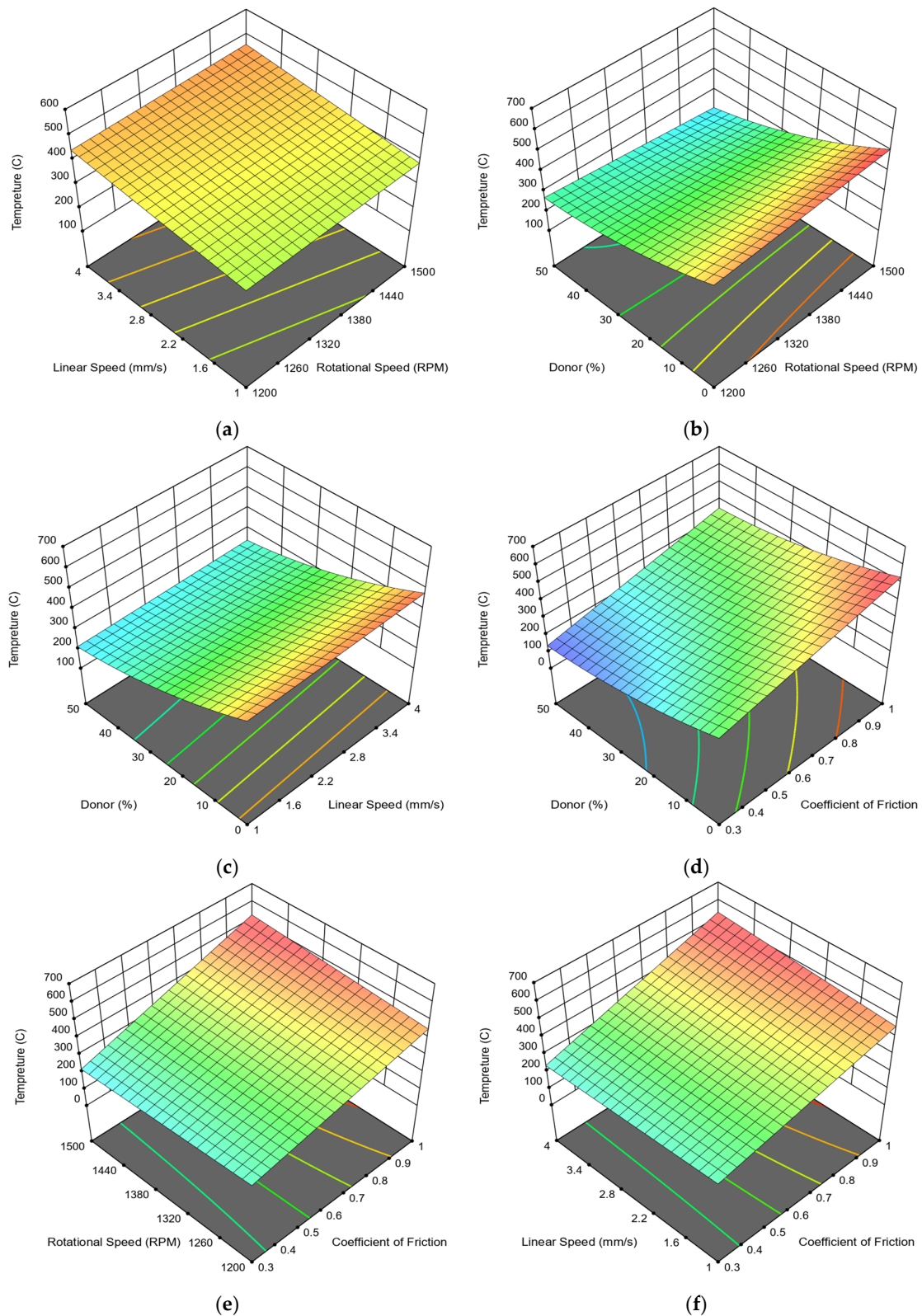


**Figure 8.** Plunge zone temperature response to varying input factors in FSW. (a) Temperature versus the rotational and transverse speeds. (b) Temperature against the Cu donor material percentage and rotational speed. (c) Temperature against the Cu donor material percentage and transverse speed. (d) Temperature against the Cu donor material percentage and the coefficient of friction. (e) Temperature against the rotational speed and the coefficient of friction. (f) Temperature against the transverse speed and the coefficient of friction.

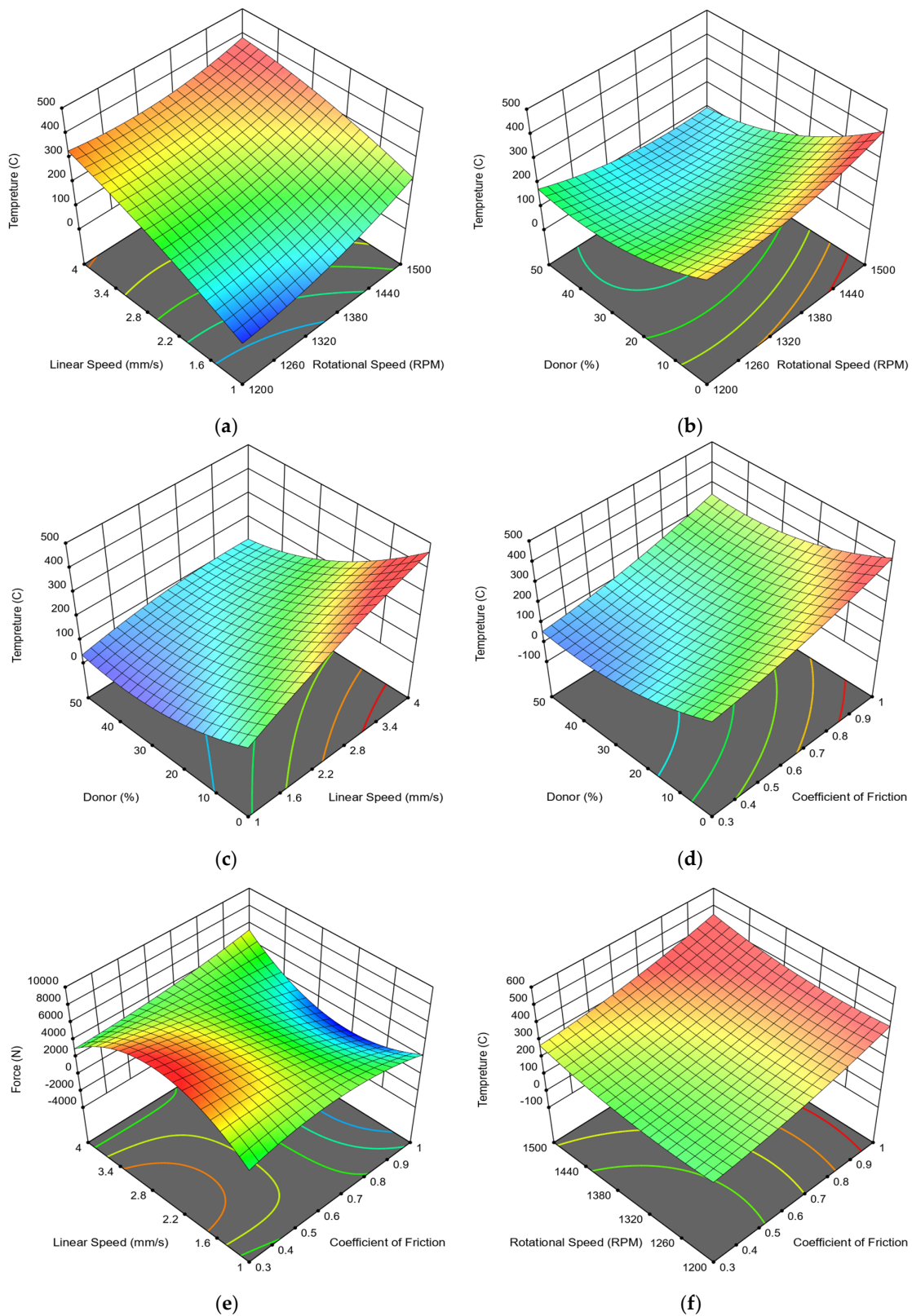


**Figure 9.** Left zone temperature response to varying input factors in FSW. (a) Temperature versus the rotational and transverse speeds. (b) Temperature against the Cu donor material percentage and rotational speed. (c) Temperature against the Cu donor material percentage and transverse speed. (d) Temperature against the Cu donor material percentage and coefficient of friction. (e) Temperature against the rotational speed and the coefficient of friction. (f) Temperature against the transverse speed and the coefficient of friction.

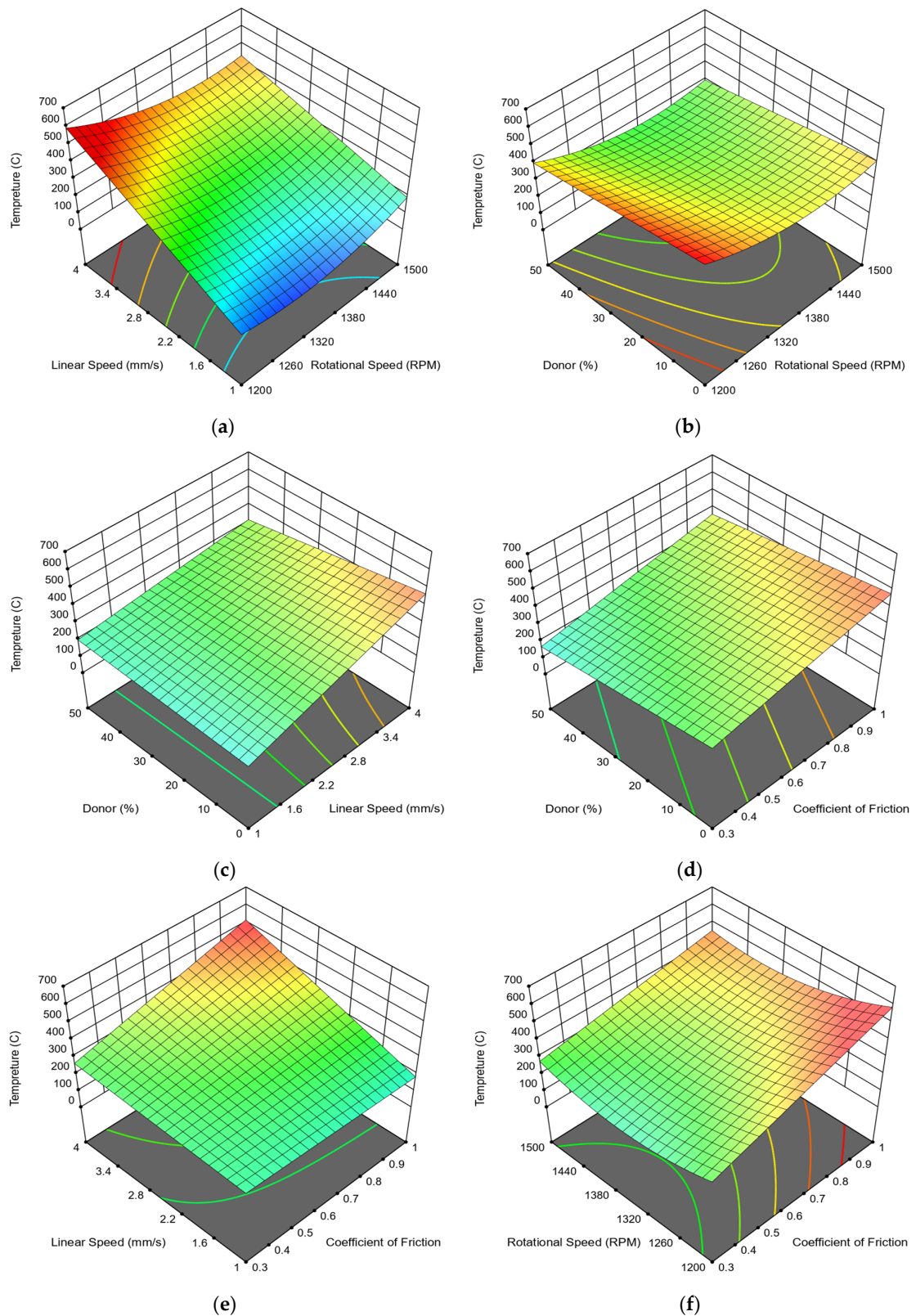


**Figure 10.** Right zone temperature response to varying input factors in FSW. (a) Temperature versus the rotational and transverse speeds. (b) Temperature against the Cu donor material percentage and rotational speed. (c) Temperature against the Cu donor material percentage and transverse speed. (d) Temperature against the Cu donor material percentage and the coefficient of friction. (e) Temperature against the rotational speed and the coefficient of friction. (f) Temperature against the transverse speed and the coefficient of friction.

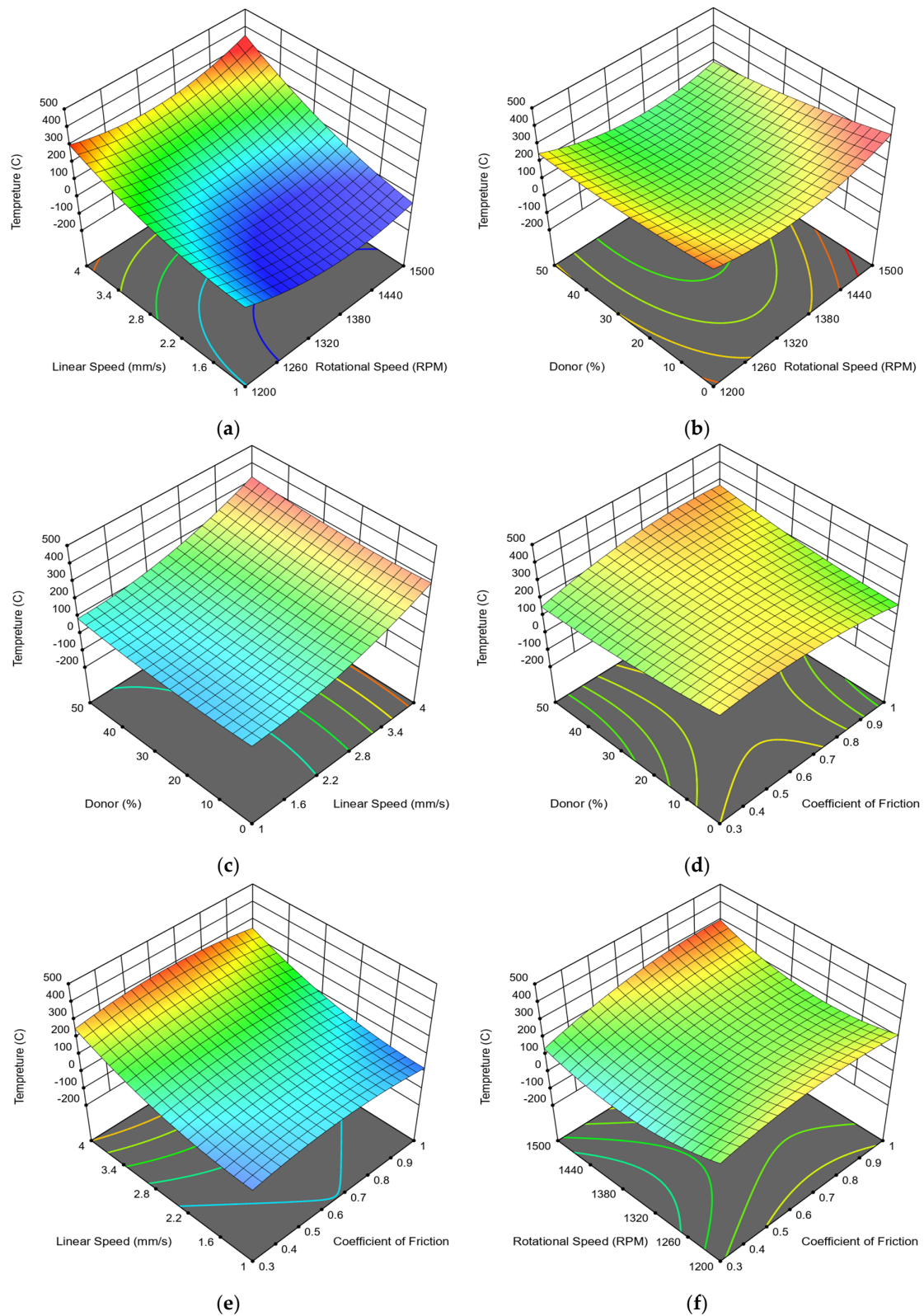


**Figure 11.** Downstream zone temperature response to varying input factors in FSW. (a) Temperature versus the rotational and transverse speeds. (b) Temperature against the Cu donor material percentage and rotational speed. (c) Temperature against the Cu donor material percentage and transverse speed. (d) Temperature against the Cu donor material percentage and the coefficient of friction. (e) Temperature against the rotational speed and the coefficient of friction. (f) Temperature against the transverse speed and the coefficient of friction.

In Figure 11a, the downstream temperature increases with a higher increase in the transverse speed, whereas the rotational speed has minimal effect. Figure 11b shows very little change in the temperature response when concurrently changing the donor percentage and the rotational speed. Figure 11c indicates that higher temperatures occur with an increase in the transverse speed, irrespective of the donor material percentage. Figure 11d shows that a moderate coefficient of friction value slightly affects the temperature results in the downstream zone. Figure 11e,f indicate that the transverse speed has more weight in increasing the temperature than the coefficient of friction and the rotational speed.

## 8. Conclusions

A comprehensive optimization analysis was conducted using Design Expert 13 software. The results from Abaqus FSW simulations were used as the input parameters, and the results were verified with experimental findings from our previous research.

The extensive factorial experiments conducted in this study revealed that the coefficient of friction was the most significant factor affecting the axial force in the plunge zone—the high F-value of 12.58 and a low value of p of 0.0062 support this notion. An increase in the coefficient of friction from 0.3 to 1.0 increased the predicted plunge force from approximately 2907 N to 3346 N.

Increasing the Cu donor material percentage from 0% to 50% decreased the plunge temperature from 502 °C to 134 °C, as supported by a low p-value of 0.0001 and a high F-value of 169.98.

The Cu donor material percentage for the left zone was highly significant, with an F-value of 339.25 and a p-value of 0.0003. In the right zone, the rotational and transverse speeds, the coefficient of friction, and the Cu donor material percentage contributed significantly to the force and temperature results. The Cu donor material percentage slightly affects the axial force and the temperature on the right and downstream zones. This is an expected outcome since the original hypothesis was based on the Cu donor material presence being restricted to the plunge zone.

The optimized parameters for each zone, identified through a multi-objective optimization process, were aimed to minimize the axial force and the control temperature for an optimized welding process. In the plunge zone, a rotational speed of 1222 rpm, a transverse speed of 1.1 mm/s, a coefficient of friction of 0.9, and a Cu donor material percentage of 19% were found optimal. In the left zone, the ideal parameters were a rotational speed of 1200 rpm, a transverse speed of 3.4 mm/s, a coefficient of friction of 0.9, and a 48% Cu donor material. For the right zone, a rotational speed of 1237 rpm, a transverse speed of 3.3 mm/s, a coefficient of friction of 0.8, and a 35% Cu donor material percentage were also optimal. A rotational speed of 1212 rpm, a transverse speed of 3.8 mm/s, a coefficient of friction of 1.0, and a 48% Cu donor material were most effective in the downstream zone. These findings offer valuable scientific insights for potential improvement in the FSW processes for high strength materials.

**Author Contributions:** Conceptualization, A.E.; methodology, S.N.B. and Z.W.; software, A.H.A.-A. and J.M.; validation, A.H.A.-A., J.M., S.N.B. and Z.W.; formal analysis, A.H.A.-A. and J.M.; investigation, S.N.B.; resources, A.E.; data curation, A.H.A.-A. and J.M.; writing—original draft preparation, A.H.A.-A. and J.M.; writing—review and editing, S.N.B. and Z.W.; supervision, A.E.; project administration, A.E.; funding acquisition, Z.W. All authors have read and agreed to the published version of the manuscript.

**Funding:** This research was funded by NASA grant number 80NSSC20M0015.

**Data Availability Statement:** The data presented in this study are available upon request from the corresponding author.

**Acknowledgments:** The authors would like to acknowledge support from NASA (award number: 80NSSC20M0015). Any opinions, findings, conclusions, or recommendations expressed in this material are those of the author(s) and do not necessarily reflect the views of NASA.

**Conflicts of Interest:** The authors declare no conflicts of interest.

### List of Symbols

AA6061-T6 aluminum alloy	
$\omega$	rotational speed (rpm)
$v$	transverse speed (mm/s)
$\mu$	coefficient of friction
D	donor material percentage (%)
$P$	axial force (N)
T	temperature ( $^{\circ}$ C)

### References

- Shankar, S.; Mehta, K.P.; Chattopadhyaya, S.; Vilaça, P. Dissimilar Friction Stir Welding of Al to Non-Al Metallic Materials: An Overview. *Mater. Chem. Phys.* **2022**, *288*, 126371. [[CrossRef](#)]
- Lakshminarayanan, A.K.; Balasubramanian, V.; Elangovan, K. Effect of Welding Processes on Tensile Properties of AA6061 Aluminium Alloy Joints. *Int. J. Adv. Manuf. Technol.* **2009**, *40*, 286–296. [[CrossRef](#)]
- Nandan, R.; DebRoy, T.; Bhadeshia, H.K.D.H. Recent Advances in Friction-Stir Welding—Process, Weldment Structure and Properties. *Prog. Mater. Sci.* **2008**, *53*, 980–1023. [[CrossRef](#)]
- Ghaffarpour, M.; Aziz, A.; Hejazi, T.-H. Optimization of Friction Stir Welding Parameters Using Multiple Response Surface Methodology. *Proc. Inst. Mech. Eng. Part L J. Mater. Des. Appl.* **2017**, *231*, 571–583. [[CrossRef](#)]
- Salah, A.N.; Mehdi, H.; Mehmood, A.; Hashmi, A.W.; Malla, C.; Kumar, R. Optimization of Process Parameters of Friction Stir Welded Joints of Dissimilar Aluminum Alloys AA3003 and AA6061 by RSM. *Mater. Today Proc.* **2022**, *56*, 1675–1683. [[CrossRef](#)]
- Pandiyarajan, R.; Marimuthu, S. Parametric Optimization and Tensile Behaviour Analysis of AA6061-ZrO<sub>2</sub>-C FSW Samples Using Box-Behnken Method. *Mater. Today Proc.* **2021**, *37*, 2644–2647. [[CrossRef](#)]
- Palanivel, R.; Koshy Mathews, P. Prediction and Optimization of Process Parameter of Friction Stir Welded AA5083-H111 Aluminum Alloy Using Response Surface Methodology. *J. Cent. South Univ.* **2012**, *19*, 1–8. [[CrossRef](#)]
- Verma, S.; Kumar, V. Optimization of Friction Stir Welding Parameters of Dissimilar Aluminium Alloys 6061 and 5083 by Using Response Surface Methodology. *Proc. Inst. Mech. Eng. C J. Mech. Eng. Sci.* **2021**, *235*, 7009–7020. [[CrossRef](#)]
- Ghaffarpour, M.; Dariani, B.M.; Hossein Kokabi, A.; Razani, N.A. Friction Stir Welding Parameters Optimization of Heterogeneous Tailored Welded Blank Sheets of Aluminium Alloys 6061 and 5083 Using Response Surface Methodology. *Proc. Inst. Mech. Eng. B J. Eng. Manuf.* **2012**, *226*, 2013–2022. [[CrossRef](#)]
- Sabry, I.; Gadallah, N.; Abu-Okail, M. Optimization of Friction Stir Welding Parameters Using Response Surface Methodology Optimization of Friction Stir Welding Parameters Using Response Surface Methodology. *IOP Conf. Ser. Mater. Sci. Eng.* **2020**, *973*, 012017. [[CrossRef](#)]
- Madani, T.; Boukraa, M.; Aissani, M.; Chekifi, T.; Ziadi, A.; Zirari, M. Experimental Investigation and Numerical Analysis Using Taguchi and ANOVA Methods for Underwater Friction Stir Welding of Aluminium Alloy 2017 Process Improvement. *Int. J. Press. Vessel. Pip.* **2023**, *201*, 104879. [[CrossRef](#)]
- Tinguery, K.M.S.; Rahem, A.; Nadeau, F.; Fafard, M. Friction Stir Welding Parameters Development of AA6061-T6 Extruded Alloy Using a Bobbin Tool. *Eng. Proc.* **2023**, *43*, 50. [[CrossRef](#)]
- Iqbal, M.P.; Tripathi, A.; Jain, R.; Mahto, R.P.; Pal, S.K.; Mandal, P. Numerical Modelling of Microstructure in Friction Stir Welding of Aluminium Alloys. *Int. J. Mech. Sci.* **2020**, *185*, 105882. [[CrossRef](#)]
- Schmidt, H.; Hattel, J. A Local Model for the Thermomechanical Conditions in Friction Stir Welding. *Model Simul. Mat. Sci. Eng.* **2005**, *13*, 77. [[CrossRef](#)]
- Maneiah, D.; Mishra, D.; Rao, K.P.; Raju, K.B. Process Parameters Optimization of Friction Stir Welding for Optimum Tensile Strength in Al 6061-T6 Alloy Butt Welded Joints. *Mater. Today Proc.* **2020**, *27*, 904–908. [[CrossRef](#)]
- Chalurkar, C.; Shukla, D.K. Temperature Analysis of Friction Stir Welding (AA6061-T6) with Coupled Eulerian-Lagrangian Approach. *IOP Conf. Ser. Mater. Sci. Eng.* **2022**, *1248*, 012035. [[CrossRef](#)]
- Sharma, Y.; Singh, K.J.; Vasudev, H. Experimental Studies on Friction Stir Welding of Aluminium Alloys. *Mater. Today Proc.* **2022**, *50*, 2387–2391. [[CrossRef](#)]
- Sefene, E.M.; Tsai, Y.H.; Jamil, M.; Jatti, V.S.; Mishra, A.; AsmareTsegaw, A.; Costa, E.C. A Multi-Criterion Optimization of Mechanical Properties and Sustainability Performance in Friction Stir Welding of 6061-T6 AA. *Mater. Today Commun.* **2023**, *36*, 106838. [[CrossRef](#)]
- Raturi, M.; Bhattacharya, A. Temperature Variation and Influence on Local Mechanical Properties Assessed by Nanoindentation in AA6061-AA7075 Dissimilar FSW. *Int. Commun. Heat Mass Transf.* **2023**, *148*, 107079. [[CrossRef](#)]
- Yue, W.; Liu, H.; Meng, S.; Xiao, J.; Huang, T. An Approach for Predicting the Tool Forces in Friction Stir Welding of AA6061-T6 Aluminium Alloy. *Int. J. Adv. Manuf. Technol.* **2023**, *126*, 5289–5305. [[CrossRef](#)]
- Salih, O.S.; Ou, H.; Sun, W. Heat Generation, Plastic Deformation and Residual Stresses in Friction Stir Welding of Aluminium Alloy. *Int. J. Mech. Sci.* **2023**, *238*, 107827. [[CrossRef](#)]

22. Lu, X.; Zhang, W.; Sun, X.; Sun, S.; Liang, S.Y. A Study on Temperature Field and Process of FSW Thick 2219 Aluminum Alloy Plate. *J. Braz. Soc. Mech. Sci. Eng.* **2023**, *45*, 326. [[CrossRef](#)]
23. Jo, D.S.; Kahhal, P.; Kim, J.H. Optimization of Friction Stir Spot Welding Process Using Bonding Criterion and Artificial Neural Network. *Materials* **2023**, *16*, 3757. [[CrossRef](#)]
24. Mandal, S.; Rice, J.; Elmustafa, A.A. Experimental and Numerical Investigation of the Plunge Stage in Friction Stir Welding. *J. Mater. Process Technol.* **2008**, *203*, 411–419. [[CrossRef](#)]
25. Maniscalco, J.; Elmustafa, A.A.; Bhukya, S.; Wu, Z. Numerical Simulation of the Donor Assisted Stir Material for Friction Stir Welding of Aluminum Alloys and Carbon Steel. *Int. J. Mater. Form.* **2022**, *13*, 164. [[CrossRef](#)]
26. Bhukya, S.N.; Wu, Z.; Maniscalco, J.; Elmustafa, A. Effect of Copper Donor Material-Assisted Friction Stir Welding of AA6061-T6 Alloy on Downward Force, Microstructure, and Mechanical Properties. *Int. J. Adv. Manuf. Technol.* **2022**, *119*, 2847–2862. [[CrossRef](#)]
27. Al-Allaq, A.H.; Ojha, M.; Mohammed, Y.S.; Bhukya, S.N.; Wu, Z.; Elmustafa, A.A. Post Weld Heat Treatment Effects on Microstructure, Crystal Structure, and Mechanical Properties of Donor Stir Assisted Friction Stir Welding Material of AA6061-T6 Alloy. *Int. J. Adv. Manuf. Technol.* **2023**, *129*, 1845–1854. [[CrossRef](#)]
28. State Ease, Inc. *Design-Expert Software*, Version 13; Stat-Ease, Inc.: Minneapolis, MN, USA. Available online: <https://www.stateease.com/software/design-expert/> (accessed on 28 November 2022).

**Disclaimer/Publisher’s Note:** The statements, opinions and data contained in all publications are solely those of the individual author(s) and contributor(s) and not of MDPI and/or the editor(s). MDPI and/or the editor(s) disclaim responsibility for any injury to people or property resulting from any ideas, methods, instructions or products referred to in the content.